Title: Induction of cross-reactive antibody responses against the RBD domain of the spike protein of SARS-CoV-2 by commensal microbiota

Authors: Justus Ninnemann[1]†, Lisa Budzinski[1]†, Marina Bondareva[1,2]†, Mario Witkowski[3,4,5]†, Stefan Angermair[6]†, Jakob Kreye[3,7,8,9,10], Pawel Durek[1], S. Momsen Reincke[3,7,8], Elisa Sánchez-Sendin[7,8,9], Selin Yilmaz[1], Toni Sempert[1], Gitta Anne Heinz[1], Caroline Tizian[3,4,5], Martin Raftery[11], Günther Schönrich[11], Daria Matyushkina[12], Ivan V. Smirnov[13], Vadim M. Govorun[12], Eva Schrezenmeier[14], Thomas Dörner[1,15], Silvia Zocche[16], Edoardo Viviano[17], Katharina Johanna Sehmsdorf[14], Hyun-Dong Chang[1,18], Philipp Enghard[14], Sascha Treskatsch[6], Andreas Radbruch[1], Andreas Diefenbach[3,4,5], Harald Prüss[7,8,9], Mir-Farzin Mashreghi[1,19,20], Andrey A. Kruglov[1,2,21*]

Affiliations: [1]Deutsches Rheuma-Forschungszentrum (DRFZ), an Institute of the Leibniz Association; 10117, Berlin, Germany.

[2]Belozersky Institute of Physico-Chemical Biology and Biological Faculty, M.V. Lomonosov Moscow State University; 119234, Moscow, Russia.

[3]Berlin Institute of Health (BIH); 10178, Berlin, Germany.

[4]Laboratory of Innate Immunity, Department of Microbiology and Infection Immunology, Charité-Universitätsmedizin Berlin; 12203, Berlin, Germany.

[5]Mucosal and Developmental Immunology, Deutsches Rheuma-Forschungszentrum, an Institute of the Leibniz Association; 10117, Berlin, Germany

[6]Charité - Universitätsmedizin Berlin, Corporate Member of Freie Universität and Humboldt Universität zu Berlin, Department of Anesthesiology and Intensive Care Medicine, Charité Campus Benjamin Franklin; Berlin, Germany

[7]German Center for Neurodegenerative Diseases (DZNE) Berlin; 10117, Berlin, Germany

[8]Helmholtz Innovation Lab BaoBab (Brain Antibody-omics and B-cell Lab); 10117, Berlin, Germany

[9]Department of Neurology and Experimental Neurology, Charité-Universitätsmedizin Berlin, Corporate Member of Freie Universität Berlin, Humboldt-Universität Berlin, and Berlin Institute of Health; 10117, Berlin, Germany

[10]Department of Pediatric Neurology, Charité-Universitätsmedizin Berlin, Corporate Member of Freie Universität Berlin, Humboldt-Universität Berlin, and Berlin Institute of Health; 10117, Berlin, Germany

[11]Institute of Virology, Charité-Universitätsmedizin Berlin, corporate member of Freie Universität Berlin, Humboldt-Universität zu Berlin, and Berlin Institute of Health, Berlin, Germany.

[12]Federal Research and Clinical Center of Physical-Chemical Medicine of the Federal Medical and Biological Agency; 119435, Moscow, Russia.

[13]Shemyakin-Ovchinnikov Institute of Bioorganic Chemistry, Russian Academy of Sciences; Moscow 117997, Russia

[14]Department of Nephrology and Intensive Care Medicine,Charité - Universitätsmedizin Berlin, corporate member of Freie Universität Berlin, Humboldt-Universität zu Berlin, and Berlin Institute of Health; 10117, Berlin, Germany.
[15]Department of Rheumatology and Clinical Immunology, Charité Universitätsmedizin Berlin, corporate member of Freie Universität Berlin and Humboldt-Universität zu Berlin, Berlin, Germany.
[16]Departments of Pediatric Gastroenterology, Nephrology and Metabolic Diseases, Charité University Medicine; 10117 Berlin, Germany
[17]Charité–Universitätsmedizin Berlin, Corporate Member of Freie Universität Berlin, Humboldt-Universität zu Berlin and Berlin Institute of Health, Institute of Physiology, Center for Space Medicine and Extreme Environments Berlin; 10117, Berlin, Germany
[18]Institute of Biotechnology, Technische Universität Berlin; Berlin, Germany
[19]Department of Pediatric Pulmonology, Immunology and Critical Care Medicine, Charité-Universitätsmedizin Berlin, corporate member of Freie Universität Berlin and Humboldt- Universität zu Berlin; 10117 Berlin, Germany
[20]Department BIH Center for Regenerative Therapies (BCRT), Charité-Universitätsmedizin Berlin, corporate member of Freie Universität Berlin and Humboldt-Universität zu Berlin, Campus Virchow-Klinikum; 13353 Berlin, Germany
[21]Center for Precision Genome Editing and Genetic Technologies for Biomedicine, Engelhardt Institute of Molecular Biology, Russian Academy of Sciences; 119991, Moscow, Russia.
†-these authors equally contributed to this work
*correspondence: Dr. Andrey Kruglov e-mail: kruglov@drfz.de

Abstract: The commensal microflora is a source for multiple antigens that may induce cross-reactive antibodies against host proteins and pathogens. However, whether commensal bacteria can induce cross-reactive antibodies against SARS-CoV-2 remains unknown. Here we report that several commensal bacteria contribute to the generation of cross-reactive IgA antibodies against the receptor-binding domain (RBD) of the SARS-CoV-2 Spike protein. We identified SARS-CoV-2 unexposed individuals with RBD-binding IgA antibodies at their mucosal surfaces. Conversely, neutralising monoclonal anti-RBD antibodies recognised distinct commensal bacterial species. Some of these bacteria, such as *Streptococcus salivarius,* induced a cross-reactive anti-RBD antibodies upon supplementation in mice. Conversely, severely ill COVID-19 patients showed reduction of *Streptococcus* and *Veillonella* in their oropharynx and feces and a reduction of anti-RBD IgA at mucosal surfaces. Altogether, distinct microbial species of the human microbiota can induce secretory IgA antibodies cross-reactive for the RBD of SARS-CoV-2.

Main text

SARS-CoV-2 virus infects cells via interaction of the Spike (S) protein with the ACE2 receptor, which is expressed by various cell types [1, 2, 3]. The Spike protein of SARS-CoV-2 contains a receptor-binding domain (RBD) that mediates its interaction with ACE2 and viral entry [3, 4]. Blocking of this crucial interaction by monoclonal anti-SARS-CoV-2-RBD antibodies confers protection of the host against infection of target cells [5, 6]. Systemically distributed antibodies (mainly IgG, IgM, and IgA1) curtail virus propagation after productive infection of the host, while the presence of antigen-specific antibodies secreted at the mucosal surfaces (IgA2, IgA1, and IgM) may prevent initial infection of the host [7]. The absence of IgA2 antibodies specific for SARS-CoV-2 antigens in severely diseased COVID-19 patients has also been demonstrated [8], suggesting that mucosal anti-viral IgA antibodies may protect the host from a severe course of COVID-19. Several studies have reported the presence of RBD-binding antibodies in unexposed healthy individuals [9, 10, 11, 12, 13]. Induction of such antibodies by previous infections with common cold coronaviruses has been postulated, but this link has not been formally proven. The original antigens inducing cross-reactive RBD-binding secretory IgA antibodies have remained obscure.

IgA antibodies at mucosal surfaces are mainly induced by commensal microbiota [14]. It is estimated that the human microbiota contains several millions of genes [15], thus potentially providing a plethora of epitopes for antibodies [16]. Some of such epitopes may resemble host proteins, potentially inducing autoimmunity [17, 18, 19, 20, 21], while others may resemble proteins from other microorganisms and mediate cross-reactive immunity [17, 22]. Microbiota-induced cross-reactive immunity also provides protection against microbial infections by *Citrobacter rodentium*, *Clostridiodes difficile*, *Pseudomonas aeruginosa* [23] and by viruses like influenza [24]. Protection is mediated by increasing fitness of the innate immune system, e.g. via tonic type I IFN production [25, 26], and by cross-reactive adaptive antibody responses [23]. Interestingly, cross-reactive antibodies targeting gp41 of HIV-1 are induced by commensal microbiota [27]. Here we describe the induction of cross-reactive antibody responses targeting SARS-CoV-2 by distinct members of the oral and gut microbiota.

We initially had analysed RBD-specific IgA in the fecal supernatants of age-matched healthy individuals and severely diseased COVID-19 patients (Table S1). Two out of 12 age-matched healthy donors, previously unexposed to SARS-CoV-2, as confirmed

107 by lack of anti-NP SARS-CoV-2 IgG antibodies in their sera (Fig. S1A), did have fecal
108 IgA antibodies reactive to RBD (Fig. 1A), 10 out of 21 severely diseased COVID-19
109 patients had fecal IgA specific for Spike protein RBD of SARS-CoV-2 (Fig. 1B and Fig.
110 S1B). Considering that age is an important risk factor for the development of severe
111 COVID-19, we next determined the prevalence of RBD-binding IgA antibodies in young
112 unexposed individuals (Fig. 1C, D and Table S1). We detected RBD-binding fecal IgA
113 in approximately 50% of young healthy donors and the magnitude of the RBD-binding
114 IgA responses in feces negatively correlated with the age of the donors (Fig. 1E). Given
115 the compositional complexity of fecal supernatant, we next purified IgA antibodies and
116 tested whether the mucosal RBD-binding IgA can inhibit binding of RBD protein to the
117 ACE2 receptor, thereby potentially blocking the entry of SARS-CoV-2 into the host
118 cells. To this end, we expressed human ACE2 on 293T cells, then incubated the ACE2-
119 expressing cells with biotinylated RBD in the presence of purified mucosal IgA of
120 various healthy donors (Fig. 1F, S1C). The fraction of bound RBD was analysed by
121 flow cytometry using fluorescent streptavidin. Purified intestinal IgA from 5 out of 14
122 healthy donors inhibited RBD binding to ACE2 (Fig. 1F). Of note, complete inhibition
123 of ACE2-RBD interaction was not achieved even at 1:1 dilution, indicating a rather low
124 concentration of neutralising anti-RBD IgA in the feces. Also, IgA from some donors
125 with anti-RBD antibodies did not inhibit the RBD-ACE2 interaction, indicating that
126 healthy individuals may harbor both inhibitory and non-inhibitory IgA antibodies
127 directed against the RBD of SARS-CoV-2 (Fig. 1F). Interestingly, healthy donors
128 exhibited IgA2 antibodies specific for RBD in their feces, while severely diseased
129 COVID-19 patients lacked fecal anti-RBD IgA2, consistent with a previous report [8]
130 (Fig. 1G).

131 IgA is induced by microbiota and does bind to microbiota [28]. Thus we next analysed
132 whether RBD-binding IgA also recognizes commensal microbiota. To this end, we first
133 divided our healthy cohort (HC) in two groups based on the presence or absence of
134 RBD-binding IgA in their fecal supernatants: HC RBD-IgA^{+} and HC RBD-IgA^{-},
135 respectively, and quantified the coating of bacteria by endogenous IgA. Both donor
136 groups exhibited similar coating of their intestinal microbiota by mucosal IgA1 and IgA2
137 (Fig. 1H). To identify the bacteria binding to mucosal IgA1 and IgA2, we isolated them
138 by fluorescence-activated cell sorting and determined their taxonomic composition by
139 16S rRNA sequencing. Linear discriminant (LDA) combined with effect size (LefSE)
140 analysis revealed distinct taxonomic differences of IgA coated bacteria of RBD-IgA^{+}

141 versus RBD-IgA$^-$ healthy donors. The IgA coated bacterial fraction of RBD IgA$^+$ donors
142 were enriched for *Parabacteroides*, *Sporobacter*, *Bilophila*, and *Vagococc*us, while in
143 RBD-IgA$^-$ donors the IgA coated fraction was enriched for *Pseudomonas*, *Dorea*,
144 *Soonwooa*, *Lachnospira,* and *Bacillus* genera (Fig. 1I). These data suggest that
145 mucosal anti-RBD IgA is associated with recognition of distinct commensal microbiota
146 by mucosal IgA.

147 To directly test whether anti-RBD antibodies bind to commensal bacteria, we stained
148 the fecal microbiota of healthy individuals with neutralising anti-RBD antibodies that
149 had either been generated in immunized rabbits or that had been cloned from
150 hospitalised COVID-19 patients [29]. The neutralising rabbit antibody showed binding
151 to a significant fraction of microbiota from HC (Fig. 2A). Furthermore, out of 15
152 monoclonal neutralising antibodies derived from hospitalized COVID-19 patients (for
153 the details see [29]) only two (HK CV07-287, HL CV07-250) showed no microbiota
154 binding activity (Fig. 2B, C). The remaining antibodies recognised commensal bacteria,
155 9 of them also independently of pre-existing fecal anti-RBD IgA (Fig. 2B, C). Of note,
156 two clonally related antibodies, CV07-200 and CV07-283, showed distinct binding
157 patterns (Fig. 2C and Fig. S2). Co-staining of microbiota with rabbit and human
158 monoclonal antibodies showed that both recognize similar as well as distinct fecal
159 bacteria communities (Fig. S3). Thus, most neutralising human anti-RBD SARS-CoV-
160 2 antibodies tested in our study bind to distinct commensal bacteria.

161 To identify the bacteria recognized by neutraliing anti-RBD antibodies, we stained,
162 sorted and sequenced antibody-bound fecal bacteria from 3 healthy donors using 4
163 different anti-RBD antibodies (Fig. 2D, E). Several genera with an abundance of more
164 than 1% were bound by the respective antibodies, and the identified bacteria differed
165 among various donors (Fig. 2E), highlighting the inter-individual diversity in the
166 bacterial composition. The binding of the anti-RBD IgG antibodies to microbiota was
167 specific, since neither the secondary anti-IgG antibodies used to identify their binding
168 (Fig.2), nor human IgG antibody with different specificity showed similar binding
169 patterns towards microbiota (Fig. S3B). The monoclonal human anti-RBD antibodies
170 in particular showed reactivity towards *Bacteroides*. Some of them also recognised
171 *Clostridia* species, *Streptococci*, *Escherichia* and *Bifidobacteria* (Fig. 2E). Of the
172 genera bound by IgA of HC RBD-IgA$^+$ donors, *Parabacteroides* and *Bilophila* also
173 bound to the human anti-RBD IgG antibodies (Fig. 1I, 2E).

174 By fluorescence-activated cell sorting we isolated bacteria recognised by the human
175 anti-RBD IgG antibodies from 8 healthy donors, and cultured them using selective
176 bacterial media and anaerobic culture conditions. Individual bacterial colonies were
177 further expanded and their identity determined by 16S rRNA Sanger sequencing (Fig.
178 2F). Two *Bacilli* species, three *Streptococcus* species, two *Bifidobacterium* species,
179 two *Enterococcus* species, *Veillonella parvula* and *Acidaminococcus intestinalis* were
180 identified as bacteria bound by anti-RBD antibodies (Fig. 2F). Restaining of purified
181 cultures confirmed their recognition by anti-RBD antibodies (Fig. S4A, B). One of the
182 isolated bacterial species was *Streptococcus salivarius*, bacteria living in the
183 oropharynx, with probiotic activity. Indeed, *S. salivarius* K12, an established probiotic
184 strain, is recognized by rabbit anti-RBD antibodies (Fig. S4A). Of note, some bacterial
185 cultures showed only partial staining with anti-RBD antibodies, probably reflecting the
186 heterogeneity of bacteria during growth or community-dependent surface variability.
187 Since the main route of infection with SARS-CoV-2 is via the respiratory tract, we
188 analysed the reactivity of salivary IgA against the oropharyngeal bacteria *S. salivarius*
189 *K12*, *B. pseudocatenulatum* and *B. subtilis*. Saliva from HC RBD-IgA^{+} donors
190 contained significant levels of IgA1 and IgA2 binding to *S. salivarius* and *B.*
191 *pseudocatenulatum* (Fig. S4C). Western blot analysis of bacterial lysates revealed that
192 rabbit anti-RBD antibody and the human anti-RBD IgG antibody HL CV07-200
193 recognise discrete proteins of *S. salivarius* and *B. pseudocatenulatum* which were
194 further identified by mass-spectrometry (Fig. S5A-E). Subsequent cloning and
195 overexpression in *E. coli* showed binding of anti-RBD antibody to "uncharacterised
196 protein RSSL-01370" of *S. salivarius K12* (Fig. S5B). These data demonstrate that
197 commensal microbiota express distinct protein antigens that are recognized by some,
198 but not all, neutralising anti-RBD antibodies.

199 Having shown that anti-RBD antibodies can cross-react with bacterial proteins, we
200 tested whether the bacteria expressing these proteins can induce a cross-reactive anti-
201 RBD antibody response. We immunised C57Bl/6 mice intraperitoneally once with heat-
202 killed bacteria and analysed the antibody responses against RBD 14 days later. Mice
203 immunized with heat-killed *S. salivarius*, but not those immunized with heat-killed *B.*
204 *pseudocatenulatum,* developed anti-RBD IgG antibodies in their sera (Fig. 3A).
205 *Veillonella parvulla* also induced anti-RBD IgG upon immunization (Fig. 3B). Sera from
206 mice immunised with *S. salivarius* and *V. parvulla* could inhibit the binding of RBD to
207 ACE2, as expressed in 293 T cells (Fig. 3C). Closer to the physiological situation, the

natural route of confrontation with bacteria of oropharyngeal microbiota, oral feeding with *S. salivarius K12* and *B. pseudocatenulatum*, induced fecal IgA specific for RBD in C57Bl/6 mice (Fig. 3D). Moreover, fecal supernatants from animals supplemented with bacteria inhibited binding of RBD to ACE2 (Fig. 3E). To gain further insight on the specificity of antibodies induced by oral supplementation with bacteria, we next performed epitope mapping of the IgA induced in the gut against 564 peptides derived from the Spike protein of SARS-CoV-2. We observed that both *B. pseudocatenulatum* and *S. salivarius* induced antibodies bound to the peptide sequence GFNCYFPLQSYGFQPTNGV (Fig. 3F, Fig. S6), that corresponds to the receptor binding motif (RBM) of RBD, in line with ACE2 inhibition data. Also, the peptide recognition pattern of rabbit anti-RBD and HL CV07-200 antibodies overlapped: both antibodies had in their epitopes a similar sequences within the RBM motif (Fig. S6). These data show that oral supplementation with *S. salivarius K12* and *B. pseudocatenulatum* can induce antibodies cross-reactive against the RBM motif of the spike protein of SARS-CoV-2.

In light of the ability of distinct oropharyngeal microbiota species to generate mucosal IgA cross-reactive to SARS-CoV-2, we compared the oral microbiota composition of healthy donors to that of COVID-19 patients, as well as of patients with flu-like symptoms, but negative for SARS-CoV-2 (Fig. 4 and Table S2). A principal component analysis (PCA) indicated that the oral microbiota of hospitalized COVID-19 patients differed considerably from healthy donors, patients with mild COVID-19 and patients with flu-like symptoms (Fig. 4A). First of all, the oral microbiota from severely diseased COVID-19 patients was characterized by an overall decreased bacterial diversity (Fig. 4B). A subsequent LefSE analysis revealed multiple bacterial genera enriched in severe COVID-19 patients (Fig. 4C). Conversely, *Veillonella* and *Streptococcus* genera, but not *Bifidobacteri*a genera, which we had identified as potential inducers of cross-reactive antibodies, were significantly reduced in patients with severe COVID-19 (Fig. 4C, D). Instead, these patients showed an increased abundance of the genera *Enterococcus*, *Staphylococcus* and *Escherichia/Shigella* in their oropharynx (Fig. 4C, D). This is not due to the treatment of severe COVID-19 patients with antibiotics (Abx), since our cohort includes both Abx naive and Abx-treated patients, and both groups showed the same prevalence of microbiota composition.

The differences in the oral microbiota composition also extend to the intestinal microbiota in severely affected COVID-19 patients (Fig. S7A and Table S3). Also

242 intestinal microbiota from severe COVID-19 patients displayed reduced bacterial
243 diversity (Fig. S7B) with dominance of opportunistic pathogenic bacteria, such as
244 *Enterococcus*, *Staphylococcus* and *Vagococcus* (Fig. S7C, D). *Streptococcus* genera
245 were significantly diminished in severe COVID-19 patients (Fig. S7C, D), while the
246 differences in *Bifidobacteria* genera were not significant. Thus, severe COVID-19 is
247 associated with the outgrowth of opportunistic bacteria (*Enterococci*, *Staphylococci*),
248 while other genera, like *Streptococcus* and *Veillonella* are depleted from the mucosal
249 surfaces, both oral and intestinal.

250 SARS-CoV-2 infection of human mucosal surfaces induces an inflammatory syndrome
251 that may progress towards fatal disease. Multiple factors, both host-intrinsic and host-
252 extrinsic, were uncovered as drivers of disease progression. Host-derived risk factors
253 include presence of autoantibodies against type I IFN, genetic predisposition [30, 31]
254 and preexisting disease conditions, such as diabetes, obesity, and ageing [32].
255 Furthermore, while pre-existing memory T cells specific for SARS-CoV-2 may be
256 protective, pre-existing low avidity memory T cells recognising SARS-CoV-2 antigens
257 in the elderly may be a potential risk factor during COVID-19 [8, 33]. Here we report
258 that healthy, unexposed individuals can have preexisting secretory IgA antibodies at
259 mucosal surfaces, antibodies which also bind to the RBD of the S protein of SARS-
260 CoV-2, and thus have the potential to neutralise the virus and prevent or ameliorate
261 infection and COVID-19. This pre-existing mucosal immunity fades with age.

262 Microbiota may contribute to the protection of the host from infection via modulating
263 the ACE2 receptor expression [34], induction of tonic type I IFN responses [35], and
264 via tuning systemic and mucosal TGF-β1 levels, with TGF- β1 being the inductor of
265 antibody class switch recombination to IgA [8, 36]. Here we have identified bacteria of
266 the oropharyngeal microbiota that express protein antigens on their cell surface, which
267 mimic epitopes of the RBD of the SARS-CoV-2 Spike protein, to an extent that they
268 not only are recognised by anti-RBD antibodies of different origin but can themselves
269 also trigger an antibody response capable of neutralising RBD in mice *in vivo*, both by
270 intraperitoneal immunization and by oral feeding. Presence of these bacteria is
271 associated with mucosal IgA antibodies recognizing RBD, and are capable of inhibiting
272 its binding to ACE2, in healthy donors not previously exposed to SARS-CoV-2. It
273 remains a challenge for future research, to determine how the bacteria induce such
274 antibodies. Similar observations have been reported for the HIV-1 virus [27, 37, 38].
275 In particular, a link between gp-41 and gp-120 reactive antibodies and their cross-

reactivity against microbiota has been demonstrated [27, 37]. It is evident that bacteria of the microbiota provide a rich target proteome for the mucosal immune system, and that this can result in the generation of a cross-reactive, pre-existing mucosal immunity against distinct viruses and may explain heterogeneity of human subjects in susceptibility towards viral infection.

Apart from host-intrinsic factors, the initial virus load may affect disease outcome and severity [39, 40], and there is an increasing evidence of microbiota changes during severe COVID-19 [41, 42], suggesting that the microbiota composition may be a risk factor for the development of severe disease as well [41, 42, 43]. The data are conflicting in terms of the genera associated with disease severity, which is probably due to the heterogeneity of patient cohorts and differences in treatment. A common denominator is that acute COVID-19 is associated with the prevalence of opportunistic bacteria and depletion of immunomodulatory bacteria [42]. The present study, showing an increase in *Enterococci*, *Staphylococci*, and *Vagococci*, and depletion of *Veillonella* and *Streptococc*i species in severe COVID-19 patients, is in line with this notion. But whether these changes are cause or consequence of SARS-CoV-2 infection has remained unclear.

On one hand, our data show that microbiota can be recognised by the antibodies raised against the RBD domain of the SARS-CoV-2 spike protein. Such antibodies presumably also shape the microbiota composition. Further studies analysing the impact of antibody responses induced by virus infection and vaccination induced on the microbiota composition are needed to address this fundamental question. On the other hand, immunocompromised patients and patients using immunosuppressive drugs respond poorly to the vaccination [44]. Data presented here propose that bacteria supplementation, in particular with *S. Salivarius K12*, may enhance the titers of anti-RBD IgA antibodies at the mucosal surfaces, prophylactically or therapeutically, or even in the context of vaccination.

The data presented here propose that bacterial supplementation either prophylactically, therapeutically, or in the context of vaccination, and particularly with *S. Salivarius K12*, may enhance the titers of anti-RBD IgA antibodies at the mucosal surfaces.

308 **Limitations of the study**

309 Despite of the identification of various bacteria that can induce cross-reactive immune
310 responses against the RBD domain of the SARS-CoV-2 Spike protein, it remains to be
311 determined whether induction of such antibodies in humans may protect from SARS-
312 CoV-2 infection or severe course of COVID-19. Further, the size of the cohorts used
313 in this study, both healthy and COVID-19 patients included in the study does not allow
314 for a detailed correlation analysis of microbiota-induced anti-RBD antibody responses
315 with the outcome of COVID-19.

316

317 **Materials and Methods**

318 **Human Donors**

319 The recruitment of study subjects was conducted in accordance with the Ethics
320 Committee of the Charité (EA 1/144/13 with EA 1/075/19, EA 2/066/20) and was in
321 compliance with the Declaration of Helsinki.

322

323 **Stool sample preparation**

324 Fresh stool samples of patients and healthy controls were stored on ice or at 4°C
325 before processing within 48 h. The stool was diluted in autoclaved and sterile-filtered
326 PBS (in-house, Steritop® Millipore Express®PLUS 0.22 µm, Cat. No: 2GPT05RE)
327 according to weight in the ratio 100 µg/mL and homogenized by vortex and spatula.
328 The feces solution was then subsequently filtered through 70 µm (Falcon, Cat. No.
329 352350) and 30 µm filters (CellTrics®, Sysmex, Cat. No. 04-0042-2316) and
330 centrifuged at 4000 x g to pellet the bacterial cells. The supernatant of this
331 centrifugation step was once more centrifuged at 13,000 x g to pellet residual cells.
332 The cell free supernatant was filtered through a 0.22 µm syringe top (Filtropur, Sarstedt
333 Cat. No. 83.1826.001) filter and stored at – 80°C until further use. Pellets of both
334 centrifugation steps were pooled and re-suspended in 10 mL PBS to measure the cell
335 density at 600 nm. For each working stock a cell amount resembling 0.4 OD was stored
336 in 1 mL of a 40 % glycerol in LB medium mixture in Safe Seal 2 mL reaction tubes
337 (Sarstedt, Cat. No. 72.695.500) and transferred to – 80°C.

338

339 **Swabs sample preparation**

340 Swabs were prepared for 16 S rRNA sequencing with an adapted protocol of the Quick-
341 DNA™ Fecal/Soil Microbe Miniprep Kit (Zymo Research, Cat. No. D6010). Swabs
342 were obtained from clinics on – 80 °C and kept frozen until further use. The swab stick
343 was either already stored in buffer or Bead Bashing™ buffer was added to cover the
344 swab brush. Up to 750 µL of the buffer solutions where transferred to a BashingBead™
345 Lysis Tube and rigorously mixed at 13,000 rpm at 37 °C. Following the kits protocol
346 the supernatant was harvested after centrifugation at 13,000 x g for 5 min and once
347 more filtered by an Zymo-Spin™ III-F Filter. The DNA containing solution was then
348 treated with Genomic Lysis Buffer and the containing DNA was put on a DNA binding
349 Zymo-Spin™ IICR Column repeatedly until the entire sample volume was loaded. The
350 bound DNA was washed with DNA Pre-Wash Buffer and g-DNA Wash Buffer. The
351 washed DNA was eluted in 50 µL DNA Elution buffer and once more further purified
352 by filtration through the Zymo-Spin™ III-HRC Filter. 2.5 µL of each of the prepared
353 samples was directly loaded to the amplicon PCR of the Illumina Nextera NGS protocol
354 described in the 16 s rRNA method section.

355

356 **16S rRNA gene sequencing**

357 For 16 S rRNA gene sequencing, we amplified the V3/V4 region directly from the
358 sorted samples (primer sequences: 5´-
359 TCgTCggCAgCgTCAgATgTgTATAAgAgACAgCCTACgggNggCWgCAg-3' and 5´-
360 gTCTCgTgggCTCggAgATgTgTATAAgAgACAggACTACHVgggTATCTAATCC-3')
361 with a prolonged initial heating step as described by "16S Metagenomic Sequencing
362 Library Preparation" for the Illumina MiSeq System. After the amplicon the genomic
363 DNA was removed by AmPure XP Beads (Beckman Coulter Life Science Cat. No.
364 A63881) with a 1:1.25 ratio of sample to beads (v/v). Next the amplicons were
365 checked for their size and purity on a 1.5 % agarose gel and if suitable subjected to
366 the index PCR using the Nextera XT Index Kit v2 Set C/D (Illumina, FC-131-2003).
367 After index PCR the samples were cleaned again with AmPure XP Beads (Beckman
368 Coulter Life Science Cat. No. A63881) in a 1: 0.8 ratio of sample to beads (v/v).
369 Samples were then analyzed by capillary gel electrophoresis (Agilent Fragment
370 Analyzer 5200) for correct size and purity with the NGS standard sensitivity fragment

371 analysis kit (Agilent Cat. No. DF-473). Of all suitable samples a pool of 2 nM was
372 generated and loaded to the Illumina MySeq 2500 system.

373 Raw data were processed and de-multiplexed using MiSeq Reporter Software.
374 Forward and reverse reads were combined using PANDAseq 2.11 with a minimum
375 overlap of 25 bases (PMID:22333067) and classified using "classifier.jar" 2.13 from the
376 Ribosomal Database Project with a confidence cutoff of 50% (PMID: 24288368,
377 PMID: 17586664). The copy number adjusted counts were agglomerated to bacterial
378 genera, rarefied to the smallest size and alpha diversity were estimated using
379 phyloSeq 1.34 (PMID: 23630581). Principle coordinate analysis were performed using
380 Bray–Curtis dissimilarity distance using vegan 2.5-7[45].

381 The linear discriminant analysis were performed using LEfSe, based on copy number
382 adjusted counts normalized to 1M reads [46]. Raw sequence data were deposited at
383 the NCBI Sequence Read Archive (SRA) under the accession number PRJNA738291.

384

385 **Microbiota staining**

386 The frozen microbiota stocks were topped up with 1 mL of autoclaved and sterile-
387 filtered PBS to reduce glycerol toxicity while thawing. Samples were centrifuged at
388 13,000 xg for 10 min twice, the supernatant removed and the pellets re-suspended in
389 PBS and finally divided into 10 tests. All the stainings of microbiota samples were
390 performed in a DNase containing buffer (PBS/ 0.2 % BSA/25 µg/µL DNase, Sigma
391 Aldrich Cat. No. 10104159001). Staining for human immunoglobulins was performed
392 in 100 µL with 1:50 (v/v) of the detection antibodies: anti-human IgM Brilliant Violet 650
393 (clone: MHM-88, Biolegend® Cat. No. 314526), anti-human IgG PE/ Dazzle™
394 594(clone: HP6017, Biolegend® Cat. No. 409324), anti-human IgA1 Alexa Fluor 647
395 (clone: B3506B4, Southern Biotech Cat. No. 9130-31), anti-human IgA2 Alexa Fluor
396 488 (clone: A9604D2, Southern Biotech Cat. No. 9140-30). The samples were
397 incubated for 30 minutes at 4 ° C and directly topped up with 1 mL of a 5 µM Hoechst
398 33342 solution (Thermo Fischer Scientific Cat. No. 62249) for another 30 min at 4 °C.
399 For the detection of Spike protein- similar structures the samples were first incubated
400 in 50 µL containing 0.5 µg SARS-CoV-2 Spike Neutralizing Antibody (clone:
401 HA14JL2302, Sino Biological Inc. Cat. No: 40592-R001) or Neutralizing Antibody
402 isolated from COVID-19 patients for 15 min at 4 °C then washed with PBS and stained

403 again in 50 µL of the anti-Rabbit Alexa 647 (7,5µg/ml, Jackson ImmunoResearch Cat.
404 No. 111-606-144) or anti-human IgG PE/ Dazzle™ 594 (2µg/ml) which was then
405 topped up with 5 µM Hoechst 33342 solution. After Hoechst 33342 staining samples
406 were washed with PBS and centrifuged at 13,000 x g for 5 min. After removal of
407 supernatant, the samples were re-suspended in PBS/ 0.2 % BSA. The samples were
408 transferred to 5 mL round bottom tubes (Falcon, Cat. No. 352063) for acquisition.

409

410 **Microbiota Flow Cytometry**

411 We used a BD Influx® cell sorter for all cytometric investigations of the microbiota
412 samples. The sheath buffer (PBS) for the instrument was autoclaved and sterile filtered
413 (Steritop® Millipore Express®PLUS 0.22 µm, Cat. No: 2GPT05RE) before each
414 fluidics start up. The quality of each acquisition was assured by the alignment of lasers,
415 laser delays and laser intensities by Sphero™ Rainbow Particles (BD Biosciences Cat.
416 No. 559123). For sorting, the drop delay was determined prior with Accudrop Beads
417 (BD Biosciences Cat. No. 345249). Samples were acquired with an event rate below
418 15,000 events and sorted with an event rate below 10,000 events. We always recorded
419 300,000 Hoechst 33342 positive events. We sorted up to 100,000 events for
420 sequencing directly into Protein Low Bind tubes (Eppendorf Cat. No 022431102), spun
421 down the sample at 17,000 x g and replaced residual sorting buffer by DEPC treated
422 water (Invitrogen Cat. No. 46-2224). The samples were stored in approx. 10 µL at -20
423 °C until further processing. For subsequent cultivation of bacteria, we sorted directly
424 into PYG medium and transferred the cells directly into a COY anaerobic chamber.

425

426 **Bacteria culture**

427 PYG medium and plates were prepared as described by the DSMZ (German Collection
428 of Microorganisms and Cell Cultures). 300,000 events were sorted into 1 ml of PYG
429 medium and directly transferred to a COY anaerobic chamber. Sorted bacteria were
430 plated on PYG, BHI (Brain heart infusion broth, Sigma, Cat. No. 53286-100G) and
431 Fastidious agar plates (Thermo Scientific, Cat. No. 12957138) and bacteria were
432 grown for 24 hours. Colonies were picked and PYG medium, BHI broth and Schaedler
433 broth (Roth, Cat. No. 5772.1) were inoculated with colonies from the respective plates.

434 The next day, DNA was isolated and the remaining bacteria were frozen in 40%
435 glycerol LB medium in liquid nitrogen or – 80 °C.

436

437 **Sequencing from bacterial colonies**

438 For the identification of the bacterial species bound to the neutralizing anti-RBD
439 antibodies, the DNA from 200 µl of the grown bacteria was isolated with ethanol
440 precipitation. The isolated DNA was subsequently amplified by the 16S rDNA specific
441 primers LPW57 and LPW58 [47]. In brief, bacterial DNA was amplified with Taq-
442 polymerase (0.005 u/µl, Rapidozym GmbH, Cat. No. GEN-003-1000), 3.12 mM MgCl2
443 (Rapidozym GmbH), 1 X GenTherm buffer (Rapidozym GmbH), 0.25 mM dNTP mix
444 (Thermo Scientific, Cat. No. R0192) and LPW57 and LPW 58 (1µM, TIB Molbiol) for
445 35 amplification cycles in a thermocycler. The DNA product was verified by gel
446 electrophoresis and purified with the NuceloSpin Gel and PCR Clean-up Kit
447 (Macherey-Nagel, Cat. No. 740609.50). The concentration of the purified PCR product
448 was adjusted to 5 ng/µl in 15 µl and send to Sanger sequencing by Eurofins Genomics.
449 Sequence identity was determined with the Nucleotide Basic Local Alignment Search
450 Tool (BLAST) provided by NCBI.

451

452 **Enzyme-linked immunosorbent assay**

453 For the detection of antibody titers in sera and fecal supernatants 96-well plates were
454 coated with goat anti-human Ig (H+L chain) antibody (Southern Biotech, Cat. No. 2010-
455 01) or goat anti-human IgA Fab (Southern Biotech, Cat. No. 2050-01) antibody for the
456 detection of IgG, IgM and IgA respectively. After washing with 1x PBST for 30 second,
457 the plates were blocked with 200 µL of 5% PBS/BSA for 1 hour at room temperature.
458 Next, plates were washed 3 times with 200 µL of 1x PBST for 30 second at a time. The
459 sera and fecal supernatants were diluted in PBS and 100 µL were added to the plate.
460 Standards were diluted in PBS and applied to the plate: IgA1 (Genway, Cat. No.
461 E04696), IgM (Sigma, Cat. No. 18260), IgA2 (Genway, Cat. No. 50D1F7), IgG
462 (Janssen Biotech Inc.,) then the plates were incubated over night at 4°C. After that,
463 plates were washed 5 times with 200 µL of 1x PBST and detection antibodies were
464 applied: anti-human IgG-AP (ICN/Cappel, Cat No. 59289), anti-human IgM-AP (Sigma,
465 Cat. No.A3437-.25ML), anti-human IgA-AP (Sigma, Cat.No. A2043), anti-human IgA1-

466 AP (SouthernBiotech, clone: B3506B4, Cat. No. 9130-04), anti-human IgA2-AP
467 (SouthernBiotech, clone: A9604D2, Cat. No. 9140-04) and were incubated for 1 hour
468 at 37°C. Subsequently, the plates were washed 5 times with 200 µL of 1x PBST 100
469 µL of pNPP (Sigma, Cat. No. N2770) was added to each well . Reactions were stopped
470 by addition of 3M NaOH. Optical densities were measured on Spectramax (Molecular
471 devices).

472 To determine the SARS-Cov-2 specific antibody titers, 96-well plates were coated
473 overnight with either 1 µg/ml recombinant SARS-CoV-2 (2019-nCoV) Spike Protein
474 (RBD, His Tag, Sino biological, Cat. No. 40592-V08B-100) or recombinant SARS-CoV-
475 2 Nucleocapsid His Protein, CF (RnD Systems; Cat. No. 10474-CV) protein or SARS-
476 CoV-2 Spike RBM (receptor binding motif), 480-496 aa (Eurogentec; Cat. No: As-656-
477 19). Plates were washed, blocked and the administration of sera and fecal
478 supernatants were done as previously described **[8]**. To detect RBD-specific IgA, a
479 biotinylated anti-human IgA antibody (Southern Biotech, Cat. No. 2050-08) was
480 applied, followed by an incubation for 1 h at 37°C. After washing 6 times with PBST,
481 avidin-HRP (Invitrogen, Cat. No. 88-7324-88) was added and after 1 hour incubation
482 at RT and 5 times washing with PBST, Tetramethylbenzidine (TMB) Substrate
483 (Invitrogen, Cat. No. 88-7324-88) was added. The reaction was stopped by addition of
484 2N H2SO4. Optical densities were measured on Spectramax (Molecular devices).

485

486 **Epitope mapping for anti-RBD antibodies**

487 Epitope mapping was performed using peptide microarray multiwell replitope SARS-
488 CoV-2 Spike glycoprotein (SPIKE) wild type + mutations (JPT Peptide Technologies
489 GmbH; RT-MW-WCPV-S-V02). Microarray was incubated with monoclonal anti-RBD
490 antibodies (final concentration 1 mcg/ml) or mouse fecal supernatants (1:1 dilution) at
491 30 C for 1 hours with constant rotation. Slides were washed three times with TBS buffer
492 with 0,05 % Tween-20 and further incubated with anti-rabbit Alexa 647 (Jackson
493 ImmunoResearch Cat. No. 111-606-144), anti-human IgG-Alexa647 (Southern
494 Biotech; Cat. No.: 2040-31), goat anti-Mouse IgA Antibody DyLight® 650 (Bethyl
495 Laboratories; Cat.No.: A90-103D5) at 30 C for 1 hour. Samples were washed with
496 TBS-T and deionized water, dried by centrifugation. Peptide microarray was analysed
497 using microarry scanner Innoscan 710 (Innopsys). Fluorescence intensities were
498 quantified using ImagePix.

499

500 **Flow cytometric assay for analysis of ACE2-RBD interaction**

501 HEK293T cells were transfected with a plasmid expressing human ACE2 protein. Next
502 day, the proportion of transfected cells was determined by staining with biotinylated
503 RBD (Sino biologicals, Cat: 40592-V08H-B) for 30 min. The cells were washed s once
504 with PBS/ 0.2 % BSA and subsequently stained with streptavidin-FITC (Thermo
505 Fischer Scientific: Cat. No. 11-4317-87). Further transfected cells were collected and
506 incubated with biological samples for 30 min, washed twice with PBS/BSA and
507 incubated with biotinylated RBD (Sino biologicals, Cat: 40592-V08H-B) for 30 min,
508 washed once with PBS/ 0.2 % BSA and subsequently stained with streptavidin-FITC
509 (Thermo Fischer Scientific: Cat. No. 11-4317-87). Cells were washed with PBS/ 0.2
510 % BSA measured directly. Dead cell exclusion was done by DAPI. Samples were
511 acquired on a FACSCanto (BD Biosciences) and analyzed using FlowJo v10 (Tree
512 Star Inc.) analysis software.

513

514 **Mice immunizations**

515 Grown bacteria were collected, washed three times with PBS and heat-inactivated at
516 65 C for 1 hr. Heat inactivated bacteria were resuspended with final OD_{600} equals 1.0.
517 C57Bl/6 mice were injected with 200 µl of heat-killed bacteria i.p. From oral gavage,
518 live bacteria stocks were grown, washed with PBS several times, OD_{600} was adjusted
519 to 1, 200 µl of live bacteria was gavaged every second day. All animal procedures were
520 performed in accordance with Russian regulations of animal protection.

521

522 **Protein gel electrophoresis and Western blotting**

523 48 h bacterial cultures were pelleted and were resuspended in RIPA buffer containing
524 protease inhibitors cocktail (Roche, Cat. No. 11 836 145 001). Samples were sonicated
525 at 50% voltage for 5 cycles of 10 sec pulses followed by 30 sec rest on ice. After
526 sonication glass beads (MP Biomedicals, Cat. No. 6911100) were added as 1/3 of total
527 volume to the bacterial extract. Samples were vortexed for 30 sec followed by chilling
528 on ice for 30 sec (for a total of 5 cycles). Lysates were spun down for 10 min at 20,000
529 xg and supernatant was collected. For western blot analysis samples were run on 12%

530 SDS-PAGE under reducing conditions and transferred to PVDF membrane (Bio-Rad,
531 Cat. No. 1620177). SARS-CoV-2 (2019-nCoV) Spike RBD-His Recombinant Protein
532 (Sino Biological, Cat. No. 40592-V08B-100) was used as a positive control. Membrane
533 was blocked by incubation in 5% non-fat milk (Roth, Cat. No. 68514-61-4) in TBST
534 buffer for 1 h at room temperature with constant shaking. Subsequently membrane
535 was hybridized with rabbit neutralizing anti-RBD antibody (Sino Biological, Cat. No.
536 40592-R001) or human derived RBD neutralising antibodies in blocking solution for 1h
537 at room temperature with constant shaking. Membrane was then washed in TBST and
538 incubated with anti-rabbit IgG-HRP (Cell signaling, Cat. No. 7074S) or with anti-human
539 IgG-HRP (Southern Biotech, Cat. No. 2040-05) for 1 h at room temperature with
540 constant shaking. SuperSignal West Fempto Maximum Sensitivity (Thermo Fisher
541 scientific, Cat No. 34095) substrate kit was used. The signal was acquired using Chemi
542 Doc imaging system (Bio-rad).

543

544 **Mass-spectroscopy analysis of proteins**

545 The protein bands after 1D-PAGE were excised and washed twice with 100 mL of 0.1
546 M NH4HCO3 (pH 7.5) and 50% acetonitrile mixture at 50 ^{o}C until the piece of gel
547 becomes transparent. Protein cysteine bonds were reduced with 10mM DTT in 50 mM
548 NH4HCO3 for 30 min at 56 °C and alkylated with 15 mM iodoacetamide in the dark at
549 RT for 30 min. The step with adding DTT was repeated. Then gel pieces were
550 dehydrated with 100 mcl of acetonitrile, air-dried and treated by 10 mkl of 12 mg/mL
551 solution of trypsin (Trypsin Gold, Mass Spectrometry Grade, Promega) in 50 mM
552 ammonium bicarbonate for 15 h at 37°C. Peptides were extracted with 20 mcl of 0.5%
553 trifluoroacetic acid water solution for 30 min with sonication, dried in a SpeedVac
554 (Labconco) and resuspended in 3% ACN, 0.1% TFA. Aliquots (2 mcl) from the sample
555 were mixed on a steel target with 0.3 mcl of 2,5-dihydroxybenzoic acid (SigmaAldrich)
556 solution (30 mg in 400mkl of 30% acetonitrile/0.5% trifluoroacetic acid), and the droplet
557 was left to dry at room temperature. Mass spectra were recorded on the Ultraflex II
558 MALDI-ToF-ToF mass spectrometer (Bruker Daltonik, Germany) equipped with an Nd
559 laser. The [MH]+ molecular ions were measured in reflector mode, the accuracy of the
560 mass peak measurement was 0.007%. Fragment ion spectra were generated by laser-
561 induced dissociation, slightly accelerated by low-energy collision-induced dissociation,
562 using helium as a collision gas. The accuracy of the fragment ions mass peak

563 measurement was 1Da. Correspondence of the found MS/MS fragments to the
564 proteins was performed with the help of Biotools software (Bruker Daltonik, Germany)
565 and a Mascot MS/MS ion search.

566

567 **Protein expression**

568 Uncharacterised protein RSSL-01370 was amplified from the genomic DNA of
569 *Streptococcus salivarius K12* using the following primers: 5´-
570 CTCCATATGAATTTACCAAGTCACCATACAAGGG -´3 and 5´-
571 GTGGTCGACATTCACTTTTTCAGTTGCTACACC -´3 and subsequently cloned into
572 pET-21b containing *NdeI* and *XhoI* restriction sites. Next, overnight culture of the
573 selected clone was inoculated into 2xTY growth medium containing 100 µg/ml of
574 ampicillin and grown at 30 °C with constant shaking until OD600 reached 0,8. Protein
575 expression was induced by 0,6 mM of IPTG for the next 4 hours at 30 °C. Bacterial
576 lysate was prepared and analysed as described earlier.

577

578 **Purification of IgA from fecal material**

579 Human IgA was purified from fecal supernatants with Peptide M/ Agarose (InvivoGen,
580 Cat. No. gel-pdm-2) as described by the manufacturer. Peptide M/ Agarose was used
581 to prepare a column which was equilibrated with 20 mM sodium phosphate buffer (pH
582 7). Subsequently the 0.2 µM filtered fecal supernatant was applied on the column at
583 least three times. The fecal IgA was eluted from the column after a washing step with
584 20 mM sodium phosphate, with 0.1 M Glycine-HCl. The elution was neutralized with 1
585 M Tris/HCl and was concentrated via dialysis. Finally, the IgA concentration was
586 determined with a NanoDrop 2000C (Thermo Scientific) or ELISA.

587

588 **Acknowledgements:**

589 We are grateful to Timo Rückert, Lennard Ostendorf, & Marie Burns for the help in
590 blood collection, to the members of the German Rheumatism Research Center Flow
591 Cytometry Core Facility (T. Kaiser, J. Kirsch, & R. Maier) for help with FACS analysis
592 and cell sorting, and to James Cameron for his careful editing. We thank Sergei

593 Nedospasov (MSU, Moscow, Russia) and members of DRFZ B cell club for useful
594 discussions.

595 **Funding:**

596 Work was supported by DFG (TR241 A04, A.K. and B03, H.-D.C., A.R.), Dr.
597 Rolf M. Schwiete Foundation (J.N., L. B., H.-D.C.) and Russian Science Foundation
598 grants # 21-14-00223 (A.K.) and Russian Fund for Basic Research #17-00-00435
599 (V.M.G) and #17-00-00268 (A.A.K). This Work was supported by the state of Berlin
600 and the "European Regional Development Fund" to M.F.M. (ERDF 2014–2020, EFRE
601 1.8/11, Deutsches Rheuma-Forschungszentrum), the Berlin Institute of Health with the
602 Starting Grant - Multi-Omics Characterization of SARS-CoV-2 infection, Project 6
603 "Identifying immunological targets in Covid-19" to A.D. and M.F.M., by the Deutsche
604 Forschungsgemeinschaft through TRR130 P16 to A.R., H.D.C. and P17 to H.R., by
605 the European Research Council through the Advanced Grant IMMEMO (ERC-2010-
606 AdG.20100317 Grant 268978) to A.R.

607

608 **Author contributions**

609 A.K., designed the study. J.N., L. B., M. B. A.K., did most of the experiments and
610 analysed data. J.K., M. R., H.P. generated human monoclonal neutralising anti-RBD
611 antibodies. S.Y. performed IgA purification and analysis of antibody concentrations by
612 ELISA. P.D., G.H. M.-F.M., performed 16S bacteria sequencing. D.M., V.G., I.S.,
613 performed mass-spectroscopy of isolated proteins. C.T., S. A., S. T., K. S., P.E., M.W.,
614 collected samples, analysed clinical data from COVID-19 patients. M.R., G. S.,
615 performed neutralisation assay. H.-D.C., A.R., A.D., M.W., H.P., M.-F.M., A.K.
616 designed the study and contributed to the writing of the manuscript.

617 **Competing interests:** J.N., L. B., and A.K. have a pending patent application with
618 regard to utilization of commensal bacteria for induction of antiviral immune responses.

619

620 **References**

621 1 Zhou P, Yang XL, Wang XG, Hu B, Zhang L, Zhang W*, et al.* A pneumonia outbreak associated
622 with a new coronavirus of probable bat origin. Nature 2020;**579**:270-3.
623 2 Hoffmann M, Kleine-Weber H, Schroeder S, Kruger N, Herrler T, Erichsen S*, et al.* SARS-CoV-2
624 Cell Entry Depends on ACE2 and TMPRSS2 and Is Blocked by a Clinically Proven Protease Inhibitor.
625 Cell 2020;**181**:271-80 e8.

626 3 Shang J, Wan Y, Luo C, Ye G, Geng Q, Auerbach A*, et al.* Cell entry mechanisms of SARS-CoV-
627 2. Proc Natl Acad Sci U S A 2020;**117**:11727-34.
628 4 Walls AC, Park YJ, Tortorici MA, Wall A, McGuire AT, Veesler D. Structure, Function, and
629 Antigenicity of the SARS-CoV-2 Spike Glycoprotein. Cell 2020;**181**:281-92 e6.
630 5 Cao Y, Su B, Guo X, Sun W, Deng Y, Bao L*, et al.* Potent Neutralizing Antibodies against SARS-
631 CoV-2 Identified by High-Throughput Single-Cell Sequencing of Convalescent Patients' B Cells. Cell
632 2020;**182**:73-84 e16.
633 6 Ju B, Zhang Q, Ge J, Wang R, Sun J, Ge X*, et al.* Human neutralizing antibodies elicited by
634 SARS-CoV-2 infection. Nature 2020;**584**:115-9.
635 7 Renegar KB, Small PA, Jr., Boykins LG, Wright PF. Role of IgA versus IgG in the control of
636 influenza viral infection in the murine respiratory tract. J Immunol 2004;**173**:1978-86.
637 8 Ferreira-Gomes M, Kruglov A, Durek P, Heinrich F, Tizian C, Heinz GA*, et al.* SARS-CoV-2 in
638 severe COVID-19 induces a TGF-beta-dominated chronic immune response that does not target itself.
639 Nat Commun 2021;**12**:1961.
640 9 Ng KW, Faulkner N, Cornish GH, Rosa A, Harvey R, Hussain S*, et al.* Preexisting and de novo
641 humoral immunity to SARS-CoV-2 in humans. Science 2020;**370**:1339-43.
642 10 Simula ER, Manca MA, Jasemi S, Uzzau S, Rubino S, Manchia P*, et al.* HCoV-NL63 and SARS-
643 CoV-2 Share Recognized Epitopes by the Humoral Response in Sera of People Collected Pre- and
644 during CoV-2 Pandemic. Microorganisms 2020;**8**.
645 11 Majdoubi A, Michalski C, O'Connell SE, Dada S, Narpala SR, Gelinas JP*, et al.* A majority of
646 uninfected adults show pre-existing antibody reactivity against SARS-CoV-2. JCI Insight 2021.
647 12 Anderson EM, Goodwin EC, Verma A, Arevalo CP, Bolton MJ, Weirick ME*, et al.* Seasonal
648 human coronavirus antibodies are boosted upon SARS-CoV-2 infection but not associated with
649 protection. Cell 2021.
650 13 Sokal A, Chappert P, Barba-Spaeth G, Roeser A, Fourati S, Azzaoui I*, et al.* Maturation and
651 persistence of the anti-SARS-CoV-2 memory B cell response. Cell 2021;**184**:1201-13 e14.
652 14 Macpherson AJ, Yilmaz B, Limenitakis JP, Ganal-Vonarburg SC. IgA Function in Relation to the
653 Intestinal Microbiota. Annu Rev Immunol 2018;**36**:359-81.
654 15 Tierney BT, Yang Z, Luber JM, Beaudin M, Wibowo MC, Baek C*, et al.* The Landscape of
655 Genetic Content in the Gut and Oral Human Microbiome. Cell Host Microbe 2019;**26**:283-95 e8.
656 16 Yang X, Xie L, Li Y, Wei C. More than 9,000,000 unique genes in human gut bacterial
657 community: estimating gene numbers inside a human body. PLoS One 2009;**4**:e6074.
658 17 Zarate-Blades CR, Horai R, Mattapallil MJ, Ajami NJ, Wong M, Petrosino JF*, et al.* Gut
659 microbiota as a source of a surrogate antigen that triggers autoimmunity in an immune privileged
660 site. Gut Microbes 2017;**8**:59-66.
661 18 Gil-Cruz C, Perez-Shibayama C, De Martin A, Ronchi F, van der Borght K, Niederer R*, et al.*
662 Microbiota-derived peptide mimics drive lethal inflammatory cardiomyopathy. Science
663 2019;**366**:881-6.
664 19 Greiling TM, Dehner C, Chen X, Hughes K, Iniguez AJ, Boccitto M*, et al.* Commensal orthologs
665 of the human autoantigen Ro60 as triggers of autoimmunity in lupus. Sci Transl Med 2018;**10**.
666 20 Ren Z, Wang Y, Duan T, Patel J, Liggett T, Loda E*, et al.* Cross-immunoreactivity between
667 bacterial aquaporin-Z and human aquaporin-4: potential relevance to neuromyelitis optica. J
668 Immunol 2012;**189**:4602-11.
669 21 Planas R, Santos R, Tomas-Ojer P, Cruciani C, Lutterotti A, Faigle W*, et al.* GDP-l-fucose
670 synthase is a CD4(+) T cell-specific autoantigen in DRB3*02:02 patients with multiple sclerosis. Sci
671 Transl Med 2018;**10**.
672 22 Bunker JJ, Erickson SA, Flynn TM, Henry C, Koval JC, Meisel M*, et al.* Natural polyreactive IgA
673 antibodies coat the intestinal microbiota. Science 2017;**358**.
674 23 Robak OH, Heimesaat MM, Kruglov AA, Prepens S, Ninnemann J, Gutbier B*, et al.* Antibiotic
675 treatment-induced secondary IgA deficiency enhances susceptibility to Pseudomonas aeruginosa
676 pneumonia. J Clin Invest 2018;**128**:3535-45.

677 24 Ichinohe T, Pang IK, Kumamoto Y, Peaper DR, Ho JH, Murray TS*, et al.* Microbiota regulates
678 immune defense against respiratory tract influenza A virus infection. Proc Natl Acad Sci U S A
679 2011;**108**:5354-9.
680 25 Schaupp L, Muth S, Rogell L, Kofoed-Branzk M, Melchior F, Lienenklaus S*, et al.* Microbiota-
681 Induced Type I Interferons Instruct a Poised Basal State of Dendritic Cells. Cell 2020;**181**:1080-96 e19.
682 26 Stefan KL, Kim MV, Iwasaki A, Kasper DL. Commensal Microbiota Modulation of Natural
683 Resistance to Virus Infection. Cell 2020;**183**:1312-24 e10.
684 27 Trama AM, Moody MA, Alam SM, Jaeger FH, Lockwood B, Parks R*, et al.* HIV-1 envelope gp41
685 antibodies can originate from terminal ileum B cells that share cross-reactivity with commensal
686 bacteria. Cell Host Microbe 2014;**16**:215-26.
687 28 Pabst O, Slack E. IgA and the intestinal microbiota: the importance of being specific. Mucosal
688 Immunol 2020;**13**:12-21.
689 29 Kreye J, Reincke SM, Kornau HC, Sanchez-Sendin E, Corman VM, Liu H*, et al.* A Therapeutic
690 Non-self-reactive SARS-CoV-2 Antibody Protects from Lung Pathology in a COVID-19 Hamster Model.
691 Cell 2020;**183**:1058-69 e19.
692 30 Bastard P, Rosen LB, Zhang Q, Michailidis E, Hoffmann HH, Zhang Y*, et al.* Autoantibodies
693 against type I IFNs in patients with life-threatening COVID-19. Science 2020;**370**.
694 31 Zeberg H, Paabo S. The major genetic risk factor for severe COVID-19 is inherited from
695 Neanderthals. Nature 2020;**587**:610-2.
696 32 Zhou F, Yu T, Du R, Fan G, Liu Y, Liu Z*, et al.* Clinical course and risk factors for mortality of
697 adult inpatients with COVID-19 in Wuhan, China: a retrospective cohort study. Lancet
698 2020;**395**:1054-62.
699 33 Bacher P, Rosati E, Esser D, Martini GR, Saggau C, Schiminsky E*, et al.* Low-Avidity CD4(+) T
700 Cell Responses to SARS-CoV-2 in Unexposed Individuals and Humans with Severe COVID-19.
701 Immunity 2020;**53**:1258-71 e5.
702 34 Geva-Zatorsky N, Sefik E, Kua L, Pasman L, Tan TG, Ortiz-Lopez A*, et al.* Mining the Human
703 Gut Microbiota for Immunomodulatory Organisms. Cell 2017;**168**:928-43 e11.
704 35 Bradley KC, Finsterbusch K, Schnepf D, Crotta S, Llorian M, Davidson S*, et al.* Microbiota-
705 Driven Tonic Interferon Signals in Lung Stromal Cells Protect from Influenza Virus Infection. Cell Rep
706 2019;**28**:245-56 e4.
707 36 Beller A, Kruglov A, Durek P, von Goetze V, Werner K, Heinz GA*, et al.* Specific microbiota
708 enhances intestinal IgA levels by inducing TGF-beta in T follicular helper cells of Peyer's patches in
709 mice. Eur J Immunol 2020;**50**:783-94.
710 37 Jeffries TL, Jr., Sacha CR, Pollara J, Himes J, Jaeger FH, Dennison SM*, et al.* The function and
711 affinity maturation of HIV-1 gp120-specific monoclonal antibodies derived from colostral B cells.
712 Mucosal Immunol 2016;**9**:414-27.
713 38 Williams WB, Liao HX, Moody MA, Kepler TB, Alam SM, Gao F*, et al.* HIV-1 VACCINES.
714 Diversion of HIV-1 vaccine-induced immunity by gp41-microbiota cross-reactive antibodies. Science
715 2015;**349**:aab1253.
716 39 Fajnzylber J, Regan J, Coxen K, Corry H, Wong C, Rosenthal A*, et al.* SARS-CoV-2 viral load is
717 associated with increased disease severity and mortality. Nat Commun 2020;**11**:5493.
718 40 Liu Y, Yan LM, Wan L, Xiang TX, Le A, Liu JM*, et al.* Viral dynamics in mild and severe cases of
719 COVID-19. Lancet Infect Dis 2020;**20**:656-7.
720 41 Yeoh YK, Zuo T, Lui GC, Zhang F, Liu Q, Li AY*, et al.* Gut microbiota composition reflects
721 disease severity and dysfunctional immune responses in patients with COVID-19. Gut 2021;**70**:698-
722 706.
723 42 Zuo T, Zhang F, Lui GCY, Yeoh YK, Li AYL, Zhan H*, et al.* Alterations in Gut Microbiota of
724 Patients With COVID-19 During Time of Hospitalization. Gastroenterology 2020;**159**:944-55 e8.
725 43 Gu S, Chen Y, Wu Z, Chen Y, Gao H, Lv L*, et al.* Alterations of the Gut Microbiota in Patients
726 with COVID-19 or H1N1 Influenza. Clin Infect Dis 2020.
727 44 Rincon-Arevalo H CM, Stefanski AL, Halleck F, Weber U, Szelinski F, Jahrsdörfer B,
728 Schrezenmeier H, Ludwig C, Sattler A, Kotsch K, Potekhin A, Chen Y, Burmester GR, Eckardt KU,
729 Guerra GM, Durek P, Heinrich F, Ferreira-Gomes M, Radbruch A, Budde K, Lino AC, Mashreghi MF,

730 Schrezenmeier E, Dörner T. Impaired humoral immunity to SARS-CoV-2 BNT162b2 vaccine in kidney
731 transplant recipients and dialysis patients. Science Immunology 2021.
732 45 Jari Oksanen FGB, Michael Friendly, Roeland Kindt, Pierre Legendre, Dan McGlinn, Peter R.
733 Minchin, R.B. O'Hara, Gavin L. Simpson, Peter Solymos, M. Henry H. Stevens, Eudard Szoecs, Helene
734 Wagner. vegan: Community Ecology Package. 2020.
735 46 Segata N, Izard J, Waldron L, Gevers D, Miropolsky L, Garrett WS*, et al.* Metagenomic
736 biomarker discovery and explanation. Genome Biol 2011;**12**:R60.
737 47 Woo PC, Leung PK, Leung KW, Yuen KY. Identification by 16S ribosomal RNA gene sequencing
738 of an Enterobacteriaceae species from a bone marrow transplant recipient. Mol Pathol 2000;**53**:211-
739 5.

740

741

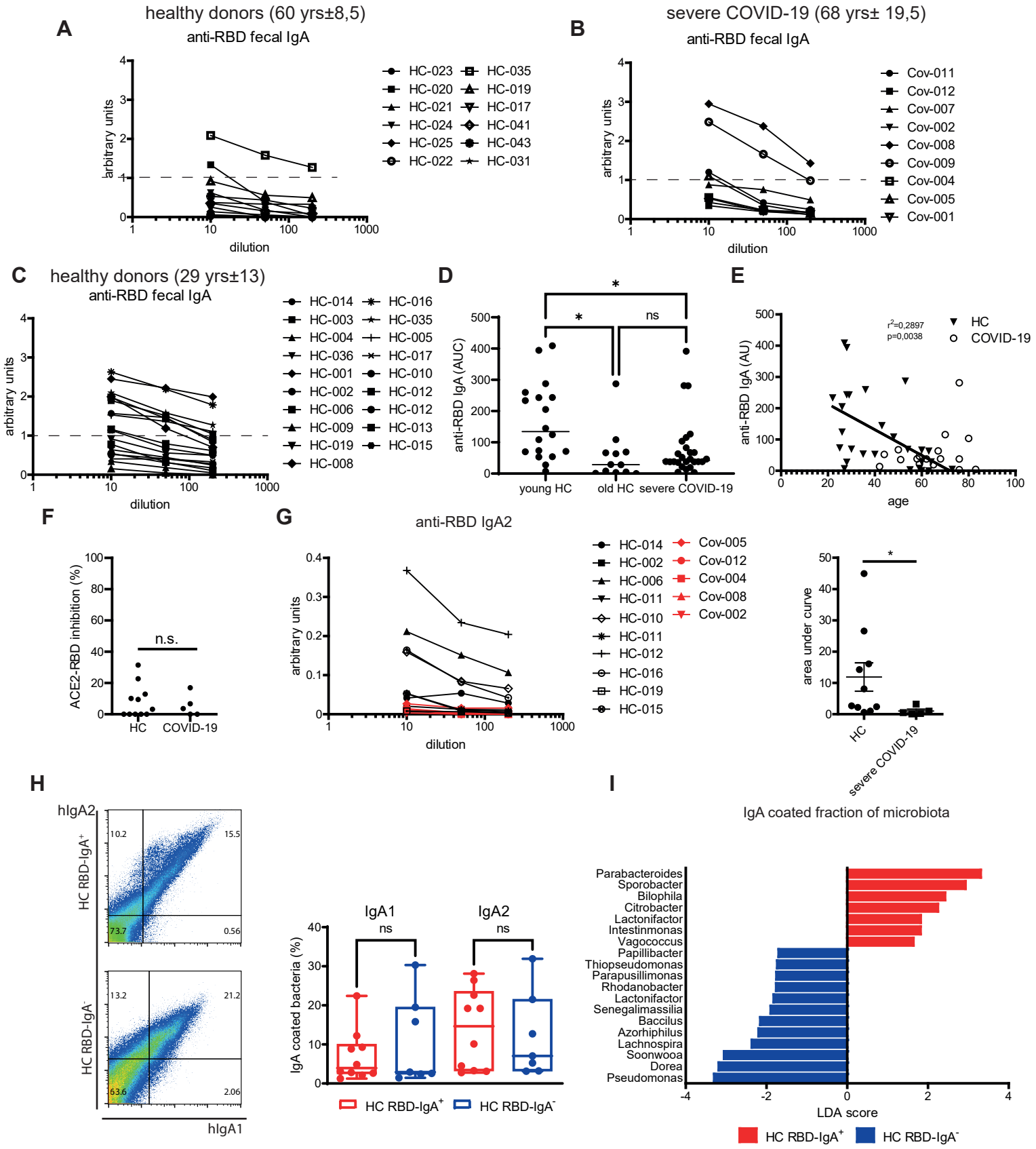

Fig. 1. Presence of mucosal IgA antibodies reactive against RBD in healthy individuals. Levels of anti-RBD IgA in fecal supernatants of age-matched healthy (**A**) and severe COVID-19 (**B**) individuals. (**C**) Levels of anti-RBD IgA in fecal supernatants of young healthy individuals. (**D**) Area under the curve (AUC) values for the anti-RBD IgA ELISA measurement of the donors presented in (**A-C**). (**E**) Correlation of the levels of anti-RBD IgA with the age in healthy individuals and COVID-19 patients. (**F**) Inhibition of RBD binding to ACE2 by IgA purified from feces of healthy people and severe COVID-19 patients. (**G**). Levels and AUC values of anti-RBD IgA2 in purified IgA fraction from healthy and severe COVID-19 individuals. (**H**). Representative dot plots and quantification of fecal IgA coating from healthy individuals that have anti-RBD IgA (HC RBD-IgA+) or lack anti-RBD IgA (HC RBD-IgA-). (**I**) Linear discriminant analysis (LDA) scores of the IgA bound bacterial fraction isolated from HC RBD-IgA+ and HC RBD-IgA-. *, $p<0.05$, **, $p<0.01$, ***, $p<0.001$, as calculated by unpaired t-test (F, G, H) or by Kruskal-Wallis test with Dunn's multiple comparisons (D); ns, not significant.

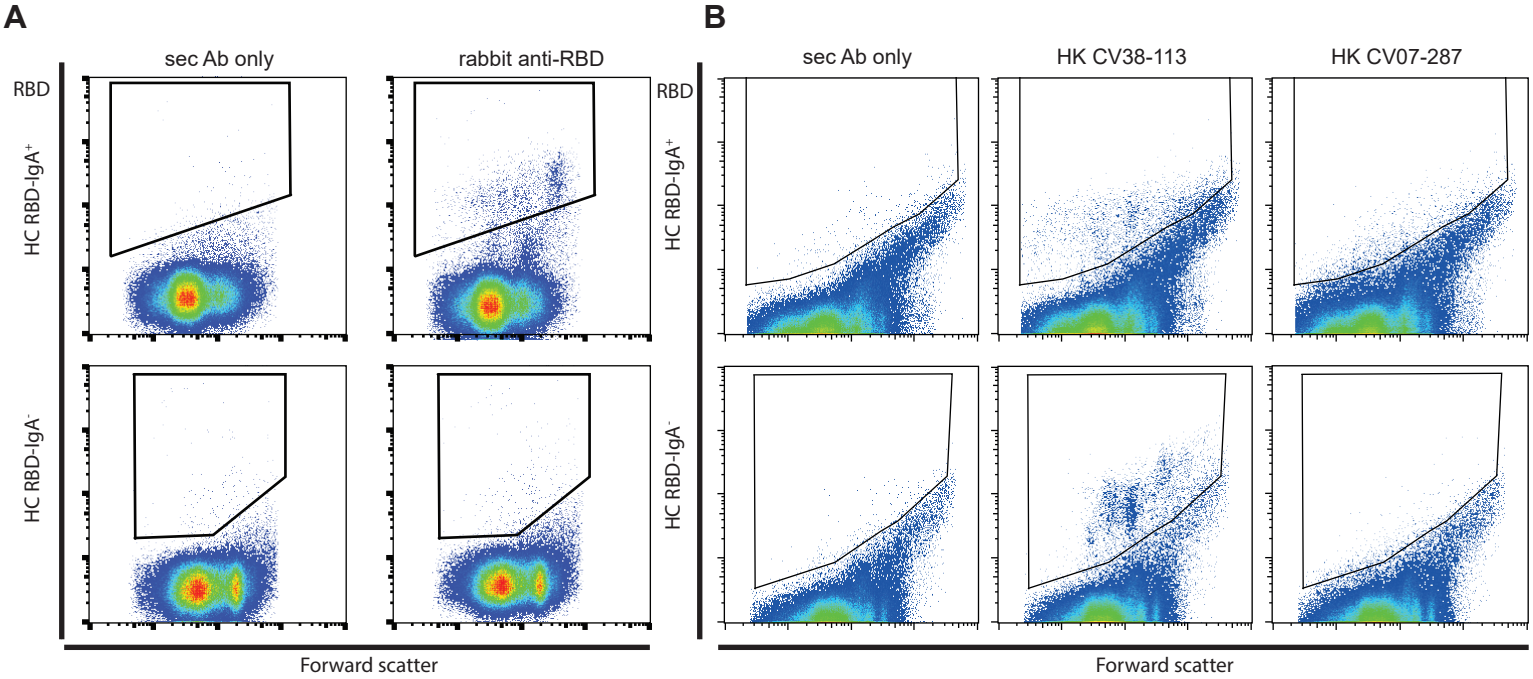

C

clone	RBD-IgA+		RBD-IgA-		
	HC-001	HC-003	HC-011	HC-009	HC-043
HK CV38-113	0	1,65	0,72	1,14	2,09
HK CV07-287	0	0	0	0	0
HL CV07-270	2,1	6,59	5,46	5,31	5,11
HK CV-X2-106	0	1,06	0	0	0
HK CV07-283	0,74	0,89	0	0	0
HL CV07-262	0,64	0,64	0	0	0
HL CV07-250	0	0	0	0	0
HL CV07-222	0,55	1,37	0	0	0
HK CV-X1-126	1,04	0,86	2,36	1,95	2
HL CV07-200	1,68	1,51	0	0	0,32
HL CV07-315	0,85	1,03	2,14	1,04	1,56
HK CV38-221	1,9	0,86	0	0	2,5
HK CV38-139	1	1,42	2,94	1,75	2,94
HK CV05-163	2,15	5,15	3,46	2,66	1,61
HL CV07-255	1,87	2,76	0	1,28	0,44
rabbit anti-RBD	1,01	3,82	0,17	0,9	0,32

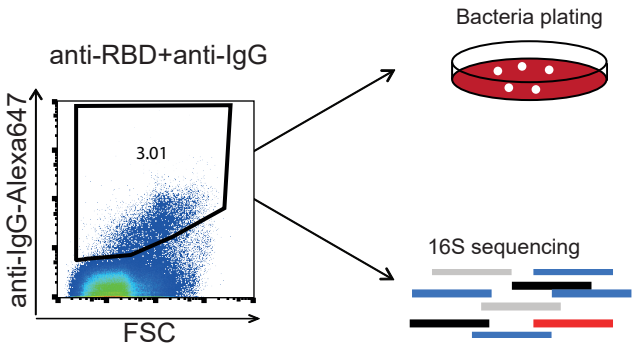

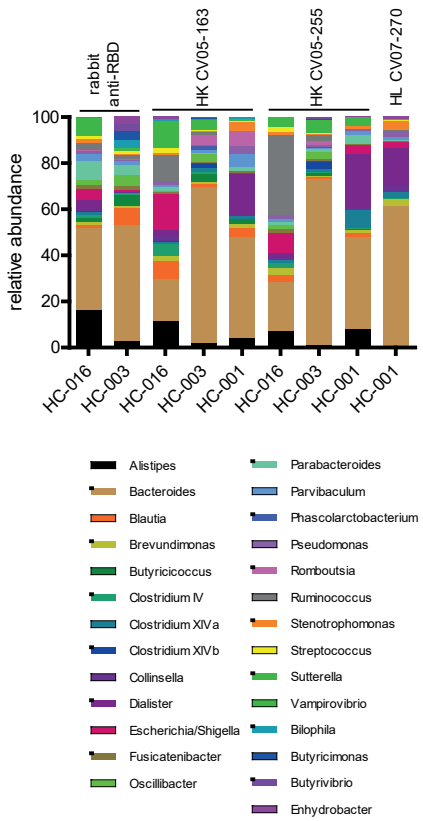

F

Bacterial strain	rabbit anti-RBD	HL CV07-270	HK CV-X1-126	HL CV07-200	HL CV07-315	HK CV05-163	HL CV07-255
Streptococcus salivarius	x	x			x		x
Sterptococcus australis/ Rubneri	x						x
Streptococcus Parasanguinis		x			x		x
Escherichia Coli	x	x			x	x	x
Bacillus safensis	x			x	x		
Bacillus cereus				x	x		
Escherichia fergusonii	x	x			x		
Bifidobacterium pseudocatenulatum		x					x
Bifidobacterium longum							x
Enterococcus Hirae		x					x
Enterococcus faecalis			x		x		
Acidaminococcus intestinalis					x		
Veillonella parvula					x		

Fig. 2. Neutralising anti-RBD antibodies recognize distinct commensal bacteria. (**A**) Representative dot plots of human fecal microbiota stained with neutralising anti-RBD antibody raised in rabbit. (**B**) Representative dot plots of microbiota stained with monoclonal neutralising anti-RBD antibodies derived from COVID-19 patients. (**C**) Frequency of bacteria bound by human neutralising anti-RBD antibodies towards microbiota from healthy individuals. Fecal microbiota from 5 heathy donors were stained with 15 monoclonal anti-RBD antibodies from COVID-19 patients or anti-rabbit RBD, followed by respective secondary fluorochrome-coupled antibodies. Bound bacterial fraction was defined via comparison of stained sample with sample stained only with secondary antibody. (**D**) Strategy for the identification of bacteria that is bound by anti-RBD antibodies. (**E**) Relative abundance of bacterial genera of greater than 1% abundance in sorted bacterial fractions bound by various anti-RBD antibodies. 16S rRNA V3-V4 region of sorted bacteria was sequenced and annotated to corresponding bacteria. Abundance was calculated in relation to the number of total reads. Genera with abundance higher than 1 % were further selected. Frequencies of selected genera were further normalized to 100%. (**F**) List of cloned bacteria isolated based on the binding to anti-RBD antibodies.

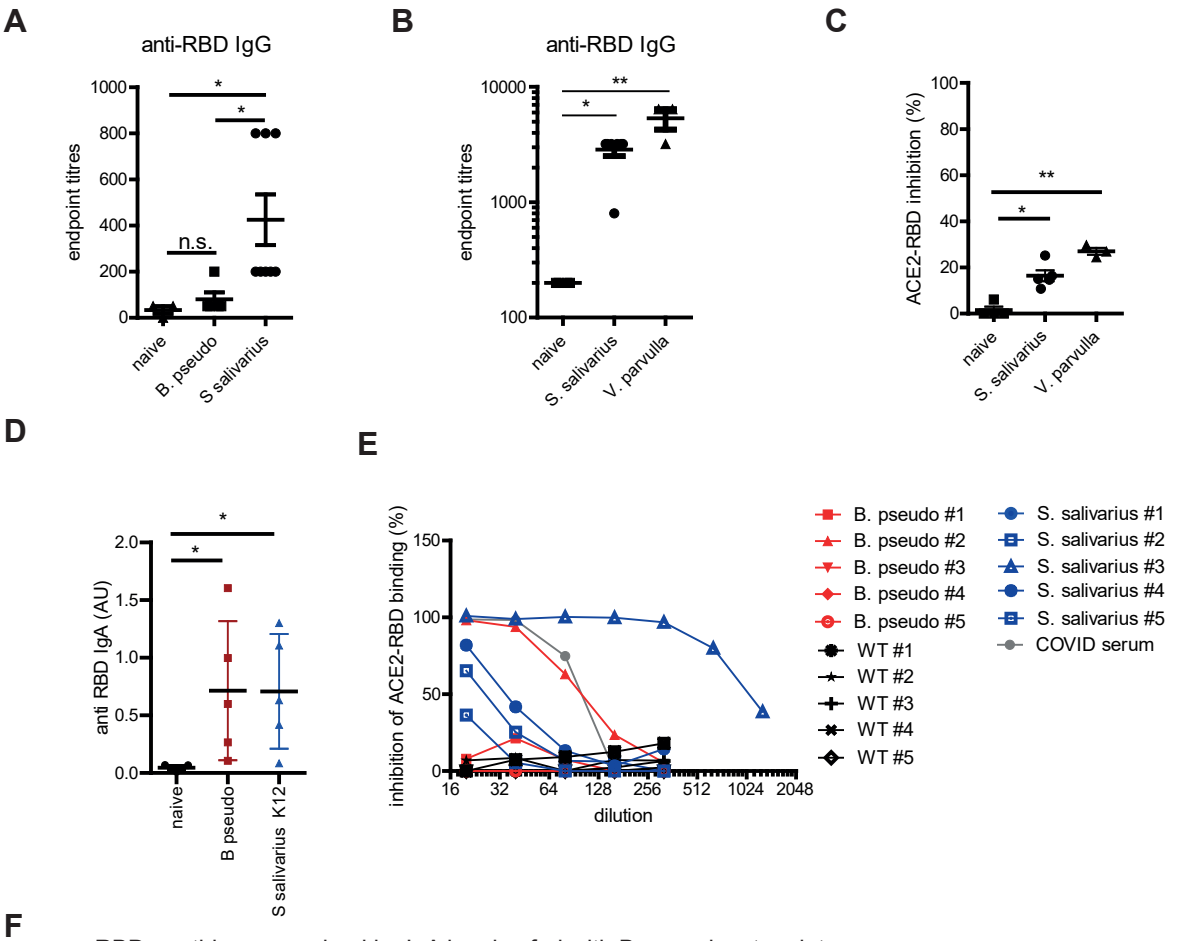

F

RBD peptides recognised by IgA in mice fed with B. pseudocatenulatum

Peptide name	Sequence	Mean fluorescent intensity
Spike-S494P_0485	GFNCYFPLQPYGFQP	58059,35
Spike-F486L_0485	GLNCYFPLQSYGFQP	39031,86
Spike-S494P_0489	YFPLQPYGFQPTNGV	39378,68
Spike_WT0485_UK0482_SA0482_BR0485_CAL0485	GFNCYFPLQSYGFQP	33629,02

RBD peptides recognised by IgA in mice fed with S. Salivarius K12

Peptide name	Sequence	Mean fluorescent intensity
Spike-F486L_0485	GLNCYFPLQSYGFQP	65535
Spike-F490S_0485	GFNCYSPLQSYGFQP	61966,04
Spike-S494P_0485	GFNCYFPLQPYGFQP	54578,13
Spike_WT0485_UK0482_SA0482_BR0485_CAL0485	GFNCYFPLQSYGFQP	64650,73
Spike-N501Y_UK0486_SA0486_BR0489	YFPLQSYGFQPTYGV	55285,27
Spike-N501T_0489	YFPLQSYGFQPTTGV	53800,07

Fig. 3. Commensal microbiota species can induce neutralising anti-RBD response. (**A**) anti-RBD IgG titers at day 14 in mice immunized with heat-killed S. salivarius and B. pseudocatenulatum. Mice were immunized as described in materials and methods. (**B**) anti-RBD IgG titers in mice immunized with isolated, heat-killed V. parvulla and S. salivarius K12. (**C**) Inhibition of RBD binding to ACE2 by sera from animals primed with heat-inactivated bacteria 14 days after immunization. (**D**) Induction of anti-RBD IgA response by oral bacterial supplementation. Mice were orally gavaged every second day as described in materials and methods. Anti-RBD IgA was analyzed in fecal supernatants. (**E**) Inhibition of ACE2-RBD binding by fecal supernatants from mice treated as in **D**. (**F**) RBD peptides recognized by the antibodies elicited upon oral supplementation of mice with S. salivarius K12 and B. pseudocatenulatum for 3 weeks. Kruskal-Wallis test with Dunn's multiple comparisons was used for (**C**) and (**D**). *, $p<0.05$, **, $p<0.01$, ***, $p<0.001$, ns, not significant. Two-way ANOVA with Bonferroni's correction was applied for the statistical evaluation of (A) and (B).

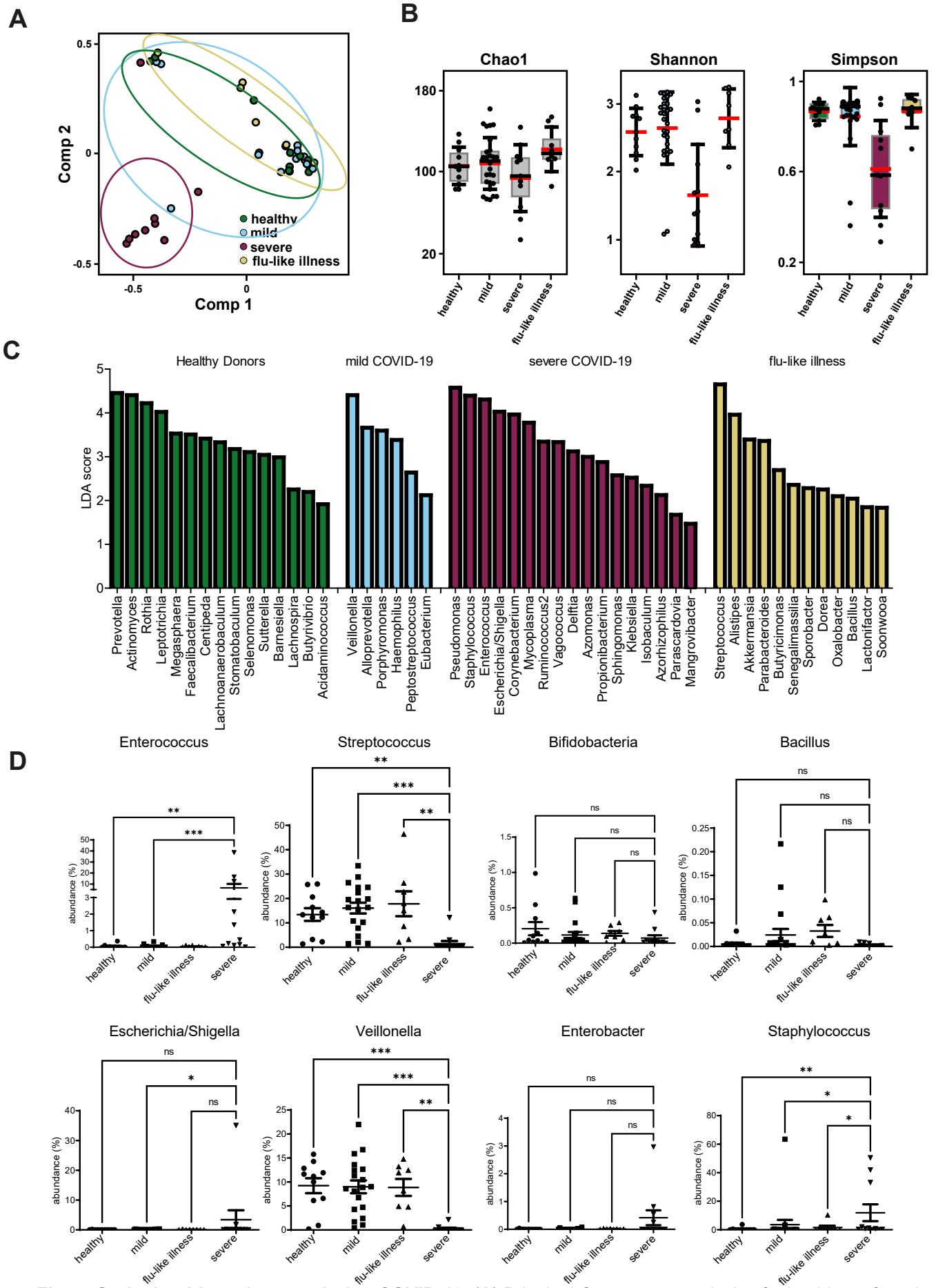

Fig. 4. Oral microbiota changes during COVID-19. (**A**) Principal Component analysis of microbiota of swabs collected from healthy individuals, mild, and severe COVID-19 patients and patients with flu-like illness. (**B**) Species richness (Chao1 index) and microbial diversity (Shannon and Simpson index) in oral microbiota collected by swabbing of healthy, mild and severe COVID-19 patients and patients with flu-like illness. (**C**) LDA scores of genera between healthy, mild and severe COVID-19 and flu-like illness. Linear discriminant analysis (LDA) combined with effect size measurements (LEfSe) was performed for 16S rRNA datasets obtained from swabs of healthy, mild and severe COVID-19 and flu-like illness. A p-value of < 0.05 was considered significant in Kruskal–Wallis test and were depicted on the figure. (**D**) Abundance of selected bacterial genera in swabs from healthy, mild and severe COVID-19 and flu-like illness. Kruskal-Wallis test with Dunn's multiple comparisons was used for (**D**) unpaired t-test was used for (**B**).
*, p<0.05, **, p<0.01, ***, p<0.001, ns, not significant.